Available online at www.sciencedirect.com
SCIENCE DIRECT®
International Journal of Heat and Mass Transfer 48 (2005) 941–955
International Journal of HEAT and MASS TRANSFER
www.elsevier.com/locate/ijhmt

Two-phase flow in high-heat-flux micro-channel heat sink for refrigeration cooling applications: Part II—heat transfer characteristics

Jaeseon Lee, Issam Mudawar *

Boiling and Two Phase Flow Laboratory, School of Mechanical Engineering, Purdue University, West Lafayette, IN 47907, United States

Received 12 July 2004; received in revised form 10 September 2004
Available online 13 November 2004

Abstract

This paper is the second of a two-part study concerning two-phase flow and heat transfer characteristics of R134a in a micro-channel heat sink incorporated as an evaporator in a refrigeration cycle. Boiling heat transfer coefficients were measured by controlling heat flux ($q'' = 15.9 - 93.8\,\mathrm{W/cm^2}$) and vapor quality ($x_e = 0.26 - 0.87$) over a broad range of mass velocity. While prior studies point to either nucleate boiling or annular film evaporation (convective flow boiling) as dominant heat transfer mechanisms in small channels, the present study shows heat transfer is associated with different mechanisms for low, medium and high qualities. Nucleate boiling occurs only at low qualities ($x_e < 0.05$) corresponding to very low heat fluxes, and high fluxes produce medium quality ($0.05 < x_e < 0.55$) or high quality ($x_e > 0.55$) flows dominated by annular film evaporation. Because of the large differences in heat transfer mechanism between the three quality regions, better predictions are possible by dividing the quality range into smaller ranges corresponding to these flow transitions. A new heat transfer coefficient correlation is recommended which shows excellent predictions for both R134a and water.

Keywords: Micro-channels; Flow boiling; Refrigeration

1. Introduction

The pioneering work by Tuckerman and Pease [1] in the early 1980s spawned unprecedented interest in the use of micro-channel heat sinks as a means for dissipating large amount of heat from small, high-flux devices in a variety of computer and aerospace applications. While their work was focused entirely on single-phase heat sinks, recent research efforts have shifted to two-phase heat sinks, which offer significant advantages compared to their single-phase counterparts. A key drawback of single-phase heat sinks is the large (and often detrimental) temperature gradient in the device resulting from a stream-wise rise in the coolant temperature. Two-phase heat sinks capitalize upon latent heat exchange, which both increases the convective heat transfer coefficient inside the heat sink and helps maintain a more uniform device surface temperature, dictated mostly by the coolant's saturation temperature.

* Corresponding author. Tel.: +1 765 494 5705; fax: +1 765 494 0539.
E-mail address: mudawar@ecn.purdue.edu (I. Mudawar).

0017-9310/$ - see front matter © 2004 Elsevier Ltd. All rights reserved.
doi:10.1016/j.ijheatmasstransfer.2004.09.019

Nomenclature

Bo	boiling number
C	two-phase multiplier parameter
Co	convection number
c_p	specific heat
d_h	hydraulic diameter
E	correlation constant
f	friction factor
Fr	Froude number
G	mass velocity [kg/m^{2}s]
g	gravitational acceleration
H_{ch}	micro-channel height
H_{tc}	distance from thermocouple to base of micro-channel
h	local heat transfer coefficient [W/m^{2}K]; enthalpy [J/kg]
k	thermal conductivity [W/m K]
L	length
m	fin parameter
M_w	molecular weight
N	correlation constant; number of experimental data
Nu	Nusselt number
P	pressure [Pa]
P_r	reduced pressure
Pr	Prandtl number
q''	heat flux through heat sink base area [W/m^2 or W/cm^2]
Re	Reynolds number based on channel hydraulic diameter
S	correlation constant
T	temperature
ΔT_{sub}	subcooling
v	specific volume [m^3/kg]
W_{ch}	micro-channel width
W_w	half-width of copper sidewall
We	Weber number
X	Martinelli parameter
X_{vt}	Martinelli parameter for laminar liquid—turbulent vapor flow
X_{vv}	Martinelli parameter for laminar liquid—laminar vapor flow
x_e	thermodynamic equilibrium quality
z	stream-wise coordinate

Greek symbols

β	ratio of channel depth to width
η	fin efficiency
μ	viscosity
ρ	density
σ	surface tension
ϕ	two-phase pressure drop multiplier

Subscripts

3	three-sided wall heating
4	four-sided wall heating
b	micro-channel base wall
c	halfway location along micro-channel
cor	correlation
exp	experiment
f	saturated liquid
fg	property difference between saturated vapor and saturated liquid
fo	liquid only
g	saturated vapor
in	channel inlet
lam	laminar
nb	nucleate boiling
out	channel outlet
pred	prediction
s	solid (copper)
sat	saturated
sp	single-phase
tp	two-phase
tur	turbulent
w	wall condition.

Despite these attributes, dissipating very large heat fluxes can lead to unacceptably high device temperatures. This is due to both the convective resistance of the coolant itself, as well as the heat diffusion resistance associated with the metallic structure of the heat sink, device and intermediate bonding agent. Avoiding high temperatures in high-flux temperature-sensitive devices can be achieved by greatly reducing the temperature of the coolant, i.e. by refrigeration. A simple means to accomplishing this goal is to incorporate the heat sink as an evaporator in a standard refrigeration cycle. This is precisely the system examined in the present study.

A key challenge to implementing this cooling scheme is the relatively poor understanding of two-phase flow and heat transfer phenomena in a micro-channel, let alone refrigerant-cooled heat sinks. The first part of the present study [2] examined the pressure drop characteristics of R134a in a two-phase heat sink and demonstrated the practical benefits of incorporating a heat sink as an evaporator in a refrigeration cycle. The present study explores the heat transfer characteristics of the same heat sink.

The dominant heat transfer mechanism inside a small channel remains an open question. Dispute over this issue is evident in several recent studies concerning boiling heat

Table 1
Summary of prior relevant mini- and micro-channel studies

Author(s)	Geometry	Fluid(s)	q'' [W/cm^2]	Flow rate	x_e	h_{tp} [W/m^{2}K]	Remarks
Lazarek and Black (1982) [3]	d=3.1 mm, L=12.3, 24.6 cm, semi-circular, single	R113	1.4–38.0	125–750 kg/m^2 s	<0–0.60	2000–10,000	h_{tp} = f(q'') nucleate boiling dominant h_{tp} independent of x_e, G
Wambsganss et al. (1993) [4]	d=2.92 mm, L = 36.8 cm, circular, single	R113	0.88–9.08	50–300 kg/m^2 s	0–0.90	1500–7000	h_{tp}=f(q'') nucleate boiling dominant h_{tp} independent of x_e,G
Bower and Mudawar (1994) [5]	d = 2.54, 0.51 mm, L=2.86 cm, circular parellel 17 micro, 3 mini	R113	3–256	45, 64 ml/min	<0–CHF		
Tran et al. (1996) [6]	d = 2.46 mm (circ.), d_h = 2.40 mm (rect.), L = 87.0 cm, single	R12	3.6–12.9	44–832 kg/m^2 s	0–0.96	2000–10,000	h_{tp} = f(q'') nucleate boiling dominant h_{tp} independent of x_e,G
Kew and Cornwell (1997) [7]	d = 1.39–3.69 mm, L = 50.0 cm circular, single	R141b	0.97–9.0	188–1480 kg/m^2 s	<0–0.95	1000–7000	h_{tp} = f(q'',x_e), h_{tp} increases with x_e nucleate and convective boiling important
Ravigururajan (1998) [8]	d_h = 0.425 mm, L = 2.052 cm, rectangular, 54 parallel	R124	8.0–65.0	75–250 ml/min	0–0.5	2000–25,000	h_{tp} = f(q'',x_e), h_{tp} increases with x_e
Yan and Lin (1998) [9]	d = 2.0 mm, L = 10.0 cm, circular, 28 parallel	R134a	0.5–2.0	50–200 kg/m^2 s	0.1–0.90	2000–6000	h_{tp} = f(q'', x_e, T_{sat})
Bao et al. (2000) [10]	d = 1.95 mm, L = 27.0 cm, circular, single	R11, R123	0.5–20.0	50–1800 kg/m^2 s	<0–0.90	3000–17,000	$h_{tp} \propto q''^{0.735}$ nucleate boiling dominant h_{tp} independent of x_e,G
Mehendale and Jacobi (2000) [11]	d_h = 0.8 mm, L = 7.4 cm, rectangular, 52 parallel	R134a	0–0.34	0–0.5 g/s	0.07–0.25	0–9000	h_{tp} = f(q'') nucleate boiling dominant h_{tp} independent of x_e,G
Lee and Lee (2001) [12]	d_h = 0.784, 6.67 mm, L = 30.0 cm, rectangular, single	R113	0.3–1.58	50–200 kg/m^2 s	0.15–0.75	1000–5000	h_{tp} = f(x_e) convective boiling dominant h_{tp} increases with x_e, q'' effect minor
Lin et al. (2001) [13]	d = 1.1 mm, L = 50.0 cm, circular, single	R141b	0.18–7.2	510 kg/m^2 s	<0–1.0	1000–6000	h_{tp} = f(q'',x_e) nucleate and convective boiling important
Yu et al. (2002) [14]	d = 2.98 mm, L = 91.0 cm, circular, single	Water–ethylene glycol	10.0–30.0	50–200 kg/m^2 s	0–1.0	8000–42,000	h_{tp} = f(q'') nucleate boiling dominant h_{tp} independent of x_e,G
Warrier et al. (2002) [15]	d_h = 0.75 mm, L = 30.74 cm, rectangular, 5 parallel	FC84	0–5.99	557–1600 kg/m^2 s	0.03–0.5		h_{tp} = f(q'', x_e)
Wen et al. (2004) [16]	d_h = 1.33 mm, L = 28.0, 24.8 cm, rectangular, single	Water	2.6–16.0	57–211 kg/m^2 s	<0–0.3	14,000– 29,000	$h_{tp} \propto q''^{0.44}$ nucleate and convective boiling important
Huo et al. (2004) [17]	d = 2.01, 4.26 mm, circular, single	R134a	1.3–15.0	100–500 kg/m^2 s	0–0.9	8000–42,000	h_{tp} = f(q'',x_e) nucleate and convective boiling important

Table 2
Contrasting features of present study compared with prior small channel boiling

	Present study	Most prior studies
Application channel geometry	Compact heat sink (cold plate) 231 μm × 713 μm L = 2.53 cm	Compact heat exchanger d_h mostly > 1 mm $L \gg 10$ cm
Heat flux	High	Low
Input heat flux	Uniform across flat surface	By external convection
Ratio of acceleration to total pressure drop	20–45%	Small to negligible
Working fluid	Environmentally-friendly refrigerant	Ozone-depleting refrigerants

transfer in mini- and micro-channels. Table 1 shows researchers are divided into two groups. The first shares the view that nucleate boiling is dominant and therefore dictates overall heat transfer inside the channel, citing the local heat transfer coefficient is dependent on heat flux, but not mass velocity or quality [3,4,6,10,11,14]. The second group shares the observation that the local heat transfer coefficient is a function of quality and mass velocity in addition to wall heat flux [7–9,12,13,15–17]. Experimental results by this second group generally show the local heat transfer coefficient decreases with increasing quality. This points to annual film evaporation (sometimes called convective boiling) as the dominant heat transfer mechanism. The discrepancy between the two groups may be explained by the different coolants, operating conditions and channel sizes used by different investigators yielding different dominant mechanisms. This important issue will be discussed later in this paper.

As indicated earlier, the primary purpose of the present paper is to explore the two-phase heat transfer characteristics of a refrigerant-cooled micro-channel heat sink. Table 2 points out the unique focus of this study compared to prior small channel refrigerant studies. While much of the existing refrigeration literature concerns long (L > 10 cm) mini-channels (d > 2 mm), the present study concerns a short heat sink (L = 25.27 mm) utilizing parallel micro-channels (231 μm × 713 μm). Furthermore, the heat sink examined in this study serves as a high-heat-flux evaporator (cold plate for electronic or power devices) subjected to a fairly uniform heat flux, while the vast majority of prior small-channel refrigeration research concerns low heat flux evaporators that are heated by external convection. It is a primary goal of the present study to develop a fundamental understanding of dominant mechanisms, and recommend an accurate method for predicting the heat transfer performance of this unique cooling scheme.

2. Experimental methods

2.1. Apparatus and measurement techniques

Fig. 1 shows the micro-channel heat sink incorporated as an evaporator in an R134a refrigeration loop. As indicated in part 1 of this study [2], the micro-channels were formed by cutting 53 of 231 μm wide and 713 μm deep micro-slots into the 25.3 × 25.3 mm^2 top surface of an oxygen-free copper block. A transparent cover plate formed a top insulating surface for the micro-channels and provided optical access to the two-phase flow inside the micro-channels. A fiberglass plastic housing surrounded the copper block and provided inlet and outlet plenums that ensured uniform flow distribution between micro-channels as well as convenient locations for inlet and outlet pressure and temperature measurement. Three cartridge heaters were embedded in the copper block and a type-K thermocouple inserted halfway along the micro-channels was used to infer the micro-channel base temperature at the same stream-wise location. Additional details concerning the construction of the micro-channel test module and measurement uncertainty are available in part 1 of this study [2].

2.2. Operating conditions

The refrigeration loop shown in Fig. 1 supplied a two-phase R134a mixture at the inlet to the micro-channel heat sink. This mixture was formed by throttling the flow by a manual metering valve situated upstream of the evaporator. Since the throttling process is isenthalpic, the evaporator's inlet enthalpy was set equal to the enthalpy determined from the temperature and pressure measured at the inlet to the throttling valve. The evaporator inlet vapor quality was determined from this enthalpy value and the measured evaporator inlet pressure. Mass flow rate was determined from the volumetric flow rate measured by the rotameter and density of subcooled liquid based on the temperature and pressure measured just downstream of the rotameter. The evaporator outlet quality was determined from the following energy balance:

$$x_{e,out} - x_{e,in} = \frac{4q''L}{Gd_h h_{fg}}. \quad (1)$$

Experimental operating conditions spanned the following ranges: inlet quality of $x_{e,in}$ = 0.001 − 0.25, outlet quality of $x_{e,out}$ = 0.49 − superheat, mass velocity of G = 127 − 654 kg/m^{2}s, heat flux of q'' = 159 − 938 kW/m^2 (15.9–93.8 W/cm^2), and inlet pressure of P_{in} = 1.44 − 6.60 bar.

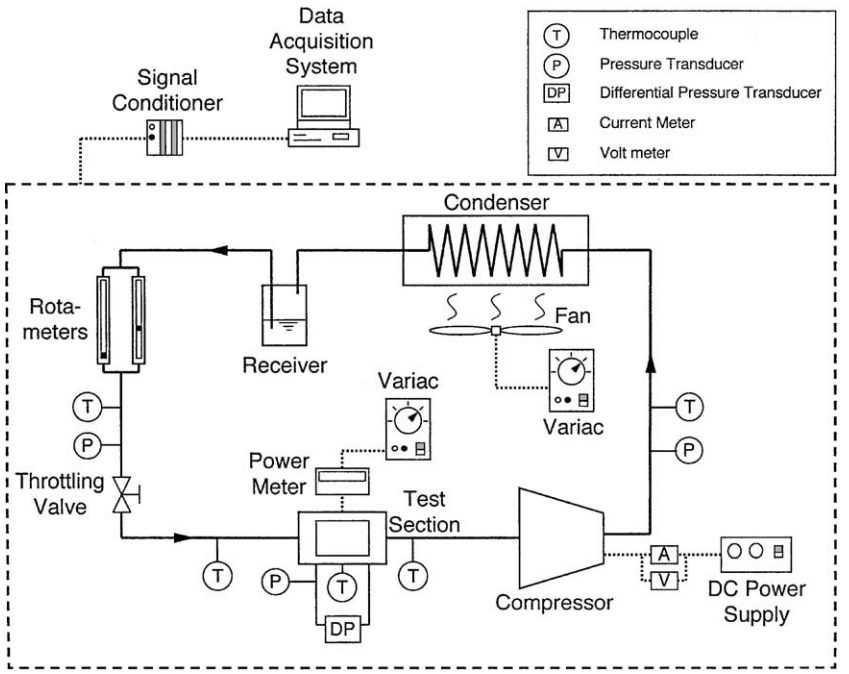

Fig. 1. Schematic of refrigeration loop.

3. Determination of heat transfer coefficient

Fig. 2 shows a unit control volume consisting of a single micro-channel and half of the surrounding copper walls. A simplified fin model of the copper walls is used to construct an energy balance for this control volume. Equating the heat influx to the unit cell through the bottom solid wall to the heat efflux by flow boiling along the micro-channel bottom and side walls (since the top wall is adiabatic) yields [18]

$$q''(W_{ch} + 2W_w) = h_{tp}(T_{w,b} - T_{f,sat})(W_{ch} + 2\eta H_{ch}), \quad (2)$$

where η is the fin efficiency. Since the top wall is adiabatic, the fin efficiency is given by [19]

$$\eta = \frac{\tanh(mH_{ch})}{mH_{ch}}, \quad (3)$$

where m is the fin parameter defined as

$$m = \sqrt{\frac{h_{tp}}{k_s W_w}}. \quad (4)$$

The fin base temperature, $T_{w,b}$, was calculated using the assumption of one-dimensional heat diffusion between the plane of the thermocouple embedded in the copper block and the plane containing the fin base.

$$T_{w,b} = T_{tc} - \frac{q''H_{tc}}{k_s}. \quad (5)$$

The fluid temperature, $T_{f,sat}$, in Eq. (2) is the bulk temperature halfway along the micro-channel based on pressure at the same location determined from the

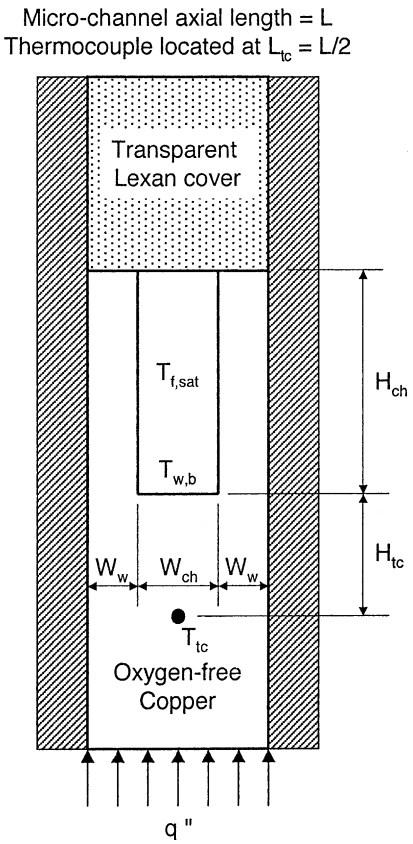

Fig. 2. Micro-channel unit cell.

measured inlet pressure and the pressure drop correlation scheme presented in part 1 of this study [2]. Calculations revealed that, excepting superheated evaporator outlet conditions, $T_{f,sat}$, was close to the mean value of the measured inlet and outlet temperatures.

Eqs. (2) and (3) are therefore used to determine h_{tp} since all other parameters are easily measured or calculated.

4. Results and discussion

4.1. Two-phase heat transfer coefficient

Fig. 3 shows the variation of the measured heat transfer coefficient h_{tp} at $z = L/2$ with quality at the same stream-wise location (obtained by substituting L in Eq. (1) by $L/2$) for different values of heat flux. This quality was varied experimentally by reducing mass flow rate (through increased throttling upstream of the evaporator) while maintaining a constant heat flux. To maintain reliable compressor operation, only values in excess of $x_{e,c} = 0.25$ could be tested. Fig. 3 shows h_{tp} decreases with increasing vapor quality, a basic feature of annular evaporative boiling, not nucleate boiling as was suggested in some of the earlier studies. Another noteworthy feature of the same data is the large magnitude of h_{tp} (2000–50,000 W/m^2 K), which is far superior to values typically attained with mini- and macro-channels.

Fig. 3 also shows the influence of heat flux on h_{tp} is very strong up to quality values around $x_{e,c} = 0.55$, beyond which there is a great diminution in the heat flux effect. For $x_{e,c} < 0.55$, the slope of h_{tp} versus $x_{e,c}$ is very steep for large heat fluxes but approaches zero at the lowest heat flux of $q'' = 15.9\,W/cm^2$. This trend points to h_{tp} values becoming constant (independent of $x_{e,c}$) had even lower heat flux values been tested. As indicated earlier, the compressor precluded operating at such low heat fluxes.

4.2. Flow visualization results

Flow visualization was used to better understand the aforementioned heat transfer coefficient trends. As indicated earlier, the transparent cover plate provided direct optical access to the boiling phenomena occurring within the micro-channel. The clarity of video and still images was limited by the small micro-channel size, lighting requirements, and internal reflection within the inner walls of the micro-channels. Fig. 4 shows an image of the flow in two adjacent micro-channels along with a schematic rendering of the same image at each of three values of quality halfway along the channel. Notice the slight differences in boiling pattern between the adjacent micro-channels. As explained in part 1 of this study [2], these differences are the result of a mild parallel channel instability causing slight flow pattern variations among the micro-channels. This form of instability was more pronounced at lower quality values.

Fig. 4(a) shows a combination of slug flow and to a lesser extent bubbly flow for $x_{ec} = 0.39$. Small bubbles exhibited violent mixing in the liquid slugs between the elongated bubbles. There are two possible sources for these small bubbles. The first is entrance inclusion since the flow enters the evaporator as a two-phase mixture. The second is nucleation within the micro-channels,

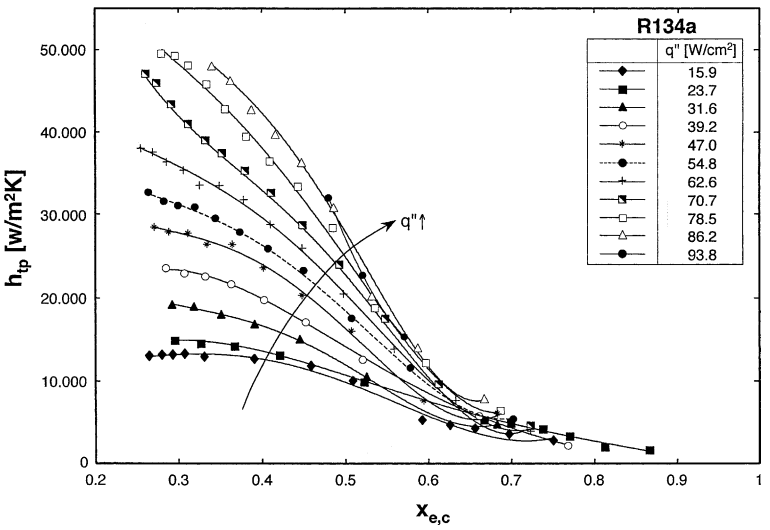

Fig. 3. Variation of local heat transfer coefficient for R134a with thermodynamic equilibrium quality for different heat fluxes.

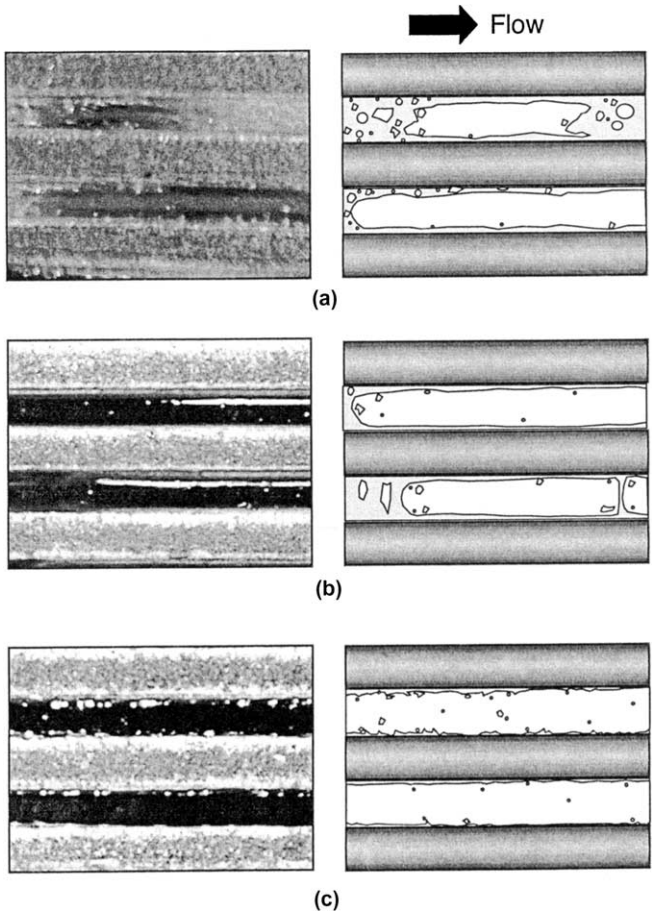

Fig. 4. Two-phase flow pattern and schematic renderings of R134a flow at (a) $x_{e,c} = 0.39$, $q'' = 31.64\,W/cm^2$, $G = 235.2\,kg/m^2s$; (b) $x_{e,c} = 0.53$, $q'' = 31.6\,W/cm^2$, $G = 163.3\,kg/m^2s$, and (c) $x_{e,c} = 0.68$, $q'' = 31.6\,W/cm^2$, $G = 128.2\,kg/m^2s$.

which can be easily detected for bubbles nucleating from the sidewalls. Previous studies with a water-cooled micro-channel heat sink showed bubbly flow could rarely be sustained [18]. In fact, annular flow was the dominant regime for most medium- and high-flux conditions. This drastic difference between two-phase flow patterns for R134a and water is explained by the low surface tension of R134a producing far smaller bubbles than in water [20]. Very small bubbles are far more apt to travel discretely along a micro-channel before coalescing into long bubbles, thus enabling the bubbly and slug flow regimes to be more prevalent in refrigerant micro-channel flow.

Fig. 4(b) shows the flow pattern at a quality value close to the transitional value discussed earlier in conjunction with the variation of h_{tp} with $x_{e,c}$, which was the upper quality boundary for a strong heat flux effect. This slug flow pattern consists mainly of elongated bubbles with very few small bubbles within the liquid slugs. Notice the two elongated bubbles in the lower micro-channel separated by a very thin liquid ridge, tending to coalesce into a single longer bubble or transition to annular flow.

Fig. 4(c) shows fully developed annular flow with a very thin liquid film covering the micro-channel walls at $x_{e,c} = 0.68$. The film appears too thin in certain locations to maintain adequate cooling. This is evident in the lower of the two micro-channels were dryout might be occurring locally, and where droplet deposition from the vapor core appears very sparse. These observations point to $x_e \approx 0.55$ as a lower boundary for local dryout, and perhaps critical heat flux (CHF) for refrigerant micro-channel flow.

Interestingly, Tran et al. [6] detected transition from slug to annular flow around $x_e \approx 0.6$–0.7, compared to $x_e \approx 0.25$–0.35 for macro-channels. The present study points to transition values smaller than those of Tran et al., but greater than for macro-channels. Clearly,

Table 3
Previous correlations for boiling in small channels

No.	Author(s)	Correlation	Remarks
1	Chen (1966) [21]	$h_{tp} = \left(\frac{Nu_3}{Nu_4}\right)(Eh_{sp} + Sh_{nb})$ $h_{sp} = Nu\frac{k_f}{d_h}, \quad Nu_{lam} = \text{const(Refer to Eq. (7) and (8))},$ $Nu_{tur} = 0.023Re_f^{0.8}Pr_f^{0.4}$ $h_{nb} = 0.00122\left(\frac{k_f^{0.79}c_{p,f}^{0.45}v_g^{0.24}}{\sigma^{0.5}\mu_f^{0.29}h_{fg}^{0.24}v_f^{0.49}}\right)\Delta T_{sat}^{0.24}\Delta P_{sat}^{0.75}$ $E = \left(1 + \frac{1}{X^{0.5}}\right)^{1.78}, \quad S = 0.9622 - -0.5822\tan^{-1}\left\{\frac{Re_f E^{1.25}}{6.18 \times 10^4}\right\}$ $X = \left[(dp/dz)_f/(dp/dz)_g\right]^{0.5}, \quad Re_f = \frac{G(1-x_e)d_h}{\mu_f}, \quad Pr_f = \frac{\mu_f c_{pf}}{k_f}$	Macro-channel correlation
2	Shah (1982) [22,23]	$h_{tp} = \left(\frac{Nu_3}{Nu_4}\right)\text{Max(E, S)}h_{sp}$ $h_{sp} = Nu\frac{k_f}{d_h}, Nu_{lam} = \text{const(Refer to Eq. (7) and (8))},$ $Nu_{tur} = 0.023Re_f^{0.8}Pr_f^{0.4}$ For $1.0 < N,\ S = 1.8/N^{0.8},\ E = 230Bo^{0.5}$ for $Bo > 3 \times 10^{-5}$ or $E = 1 + 46Bo^{0.5}$ for $Bo < 3 \times 10^{-5}$ For $0.1 < N \leqslant 1.0,\ S = 1.8/N^{0.8},\ E = FBo^{0.5}\exp(2.74N^{-0.1})$ For $N \leqslant 0.1,\ S = 1.8/N^{0.8},\ E = FBo^{0.5}\exp(2.47N^{-0.15})$, $F = 14.7$ for $Bo \geqslant 11 \times 10^{-4}$ or $F = 15.43$ for $Bo < 11 \times 10^{-4}$ $N = Co$ for $Fr_f \geqslant 0.04$ or $N = 0.38Fr_f^{-0.3}Co$ for $Fr_f < 0.04$; $Co = \left(\frac{1-x_e}{x_e}\right)^{0.8}\left(\frac{v_f}{v_g}\right)^{0.5}; \quad Fr_f = \frac{v_f^2 G^2}{gd_h}$	Macro-channel correlation
3	Liu and Winterton (1991) [24]	$h_{tp} = \left(\frac{Nu_3}{Nu_4}\right)((Eh_{sp})^2 + (Sh_{nb})^2)^{0.5}$ $h_{sp} = Nu\frac{k_f}{d_h}, Nu_{lam} = \text{const(Refer to Eq. (7) and (8))},$ $Nu_{tur} = 0.023Re_f^{0.8}Pr_f^{0.4}$ $E = \left(1 + x_e Pr_f\left(\frac{v_g}{v_f} - 1\right)\right)^{0.35}$	Macro-channel correlation

Table 3 (*continued*)

No.	Author(s)	Correlation	Remarks
		$h_{nb} = 55P_r^{0.12}(-\log_{10}(P_r))^{-0.55}M_w^{-0.5}q''^{0.67}$, $S = (1 + 0.055E^{0.1}Re_{fo}^{0.16})^{-1}$	
		If $Fr_f \leqslant 0.05$ replace E by $EFr_f^{0.1-2Fr_f}$ and S by $SFr_f^{0.5}$	
4	Lazarek and Black (1982) [3]	$h_{tp} = Nu_3[30Re_{fo}^{0.857}Bo^{0.714}]\left(\frac{k_f}{d_h}\right)$	Small channel correlation
5	Tran et al. (1996) [6]	$h_{tp} = \left(\frac{Nu_3}{Nu_4}\right)\left[8.4 \times 10^5(Bo^2We_{fo})^{0.3}\left(\frac{v_g}{v_f}\right)^{-0.4}\right]$; $We_{fo} = \frac{v_f G^2 d_h}{\sigma}$	Small channel correlation
6	Lee and Lee (2001) [12]	$h_{tp} = \left(\frac{Nu_3}{Nu_4}\right)(Eh_{sp})$	Small channel correlation
		$h_{sp} = Nu\frac{k_f}{d_h}$, $Nu_{lam} = \text{const}$(Refer to Eqs. (7) and (8)), $Nu_{tur} = 0.023Re_f^{0.8}Pr_f^{0.4}$	
		$E = 10.3\beta^{0.398}\phi_f^{0.598}$, $\phi_f^2 = 1 + \frac{C}{X} + \frac{1}{X^2}$, $C = 6.185 \times 10^{-2}Re_{fo}^{0.726}$	
		$X^2 = \left[(dp/dz)_f/(dp/dz)_g\right]$	
7	Yu et al. (2002) [14]	$h_{tp} = \left(\frac{Nu_3}{Nu_4}\right)\left[6.4 \times 10^6(Bo^2We_{fo})^{0.27}\left(\frac{v_g}{v_f}\right)^{-0.2}\right]$	Small channel correlation
8	Warrier et al. (2002) [15]	$h_{tp} = \left(\frac{Nu_3}{Nu_4}\right)(Eh_{sp})$	
		$h_{sp} = Nu\frac{k_f}{d_h}$, $Nu_{lam} = \text{const}$(Refer to Eqs. (7) and (8)), $Nu_{tur} = 0.023Re_f^{0.8}Pr_f^{0.4}$	
		$E = 1.0 + 6Bo^{1/16} + f(Bo)x_e^{0.65}$, $f(Bo) = -5.3(1 - 855Bo)$	

vapor quality is not the sole indicator for regime transition, and other parameters such surface tension and channel shape and dimensions must influence transition behavior.

5. Assessment of prior correlations

Several popular macro-channel correlations and recently recommended small-channel correlations were examined for accuracy in predicting the present heat transfer data. These correlations are summarized in Table 3. Since these correlations concern circular channels with uniform circumferential heating, predictions had to be adjusted for the three-sided wall heating and rectangular geometry of the present study using the following relation:

$$h_{tp} = h_{tp,cor}\frac{Nu_3}{Nu_4}, \tag{6}$$

where $h_{tp,cor}$ is the value predicted from a correlation, and Nu_3 and Nu_4 are the single-phase Nusselt numbers for laminar flow with three-sides and four-sides wall heating, respectively [25].

$$Nu_3 = 8.235(1 - 1.883\beta + 3.767\beta^2 - 5.814\beta^3 + 5.361\beta^4 - 2.0\beta^5) \tag{7}$$

and

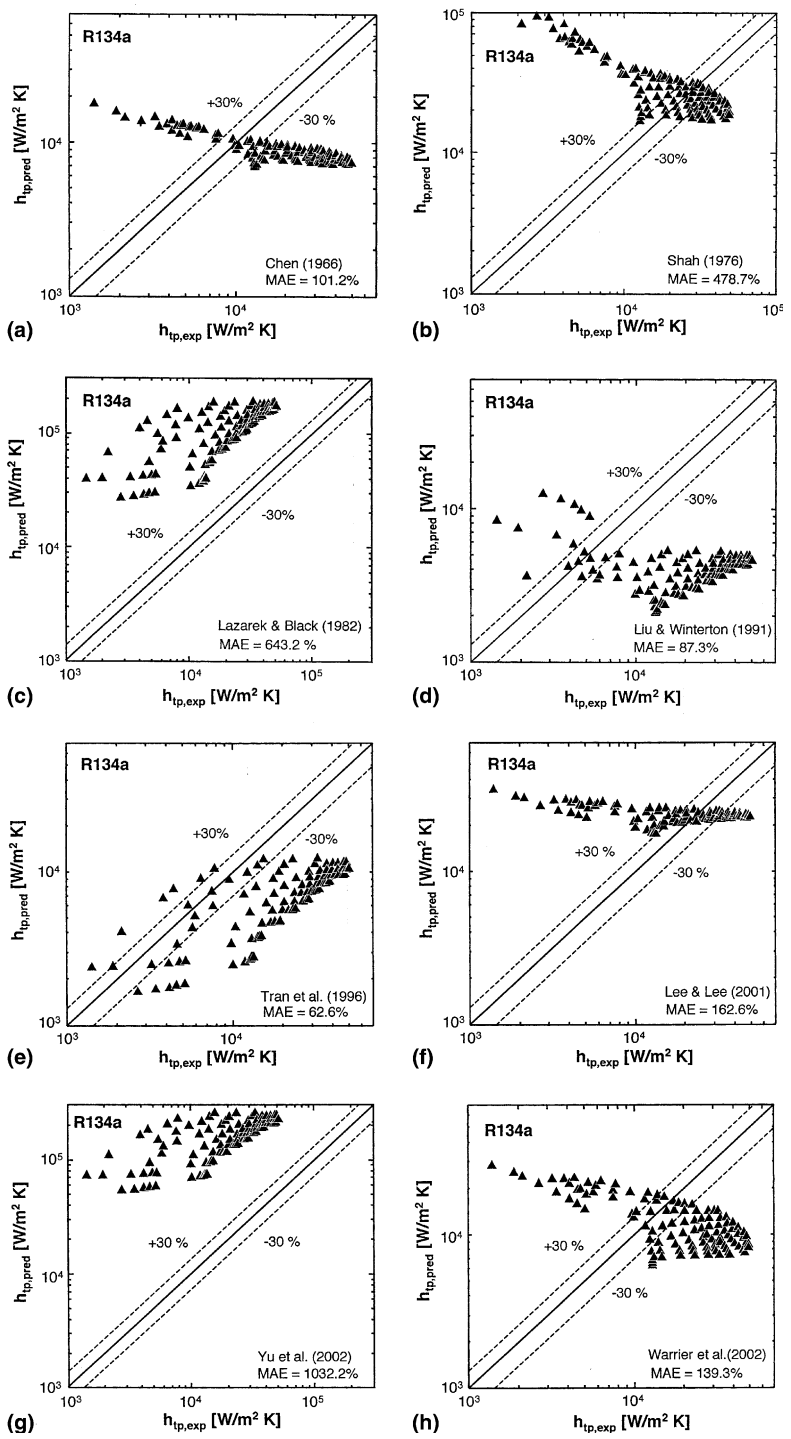

Fig. 5. Comparison of R134 a heat transfer coefficient data with predictions based on (a) Chen [21], (b) Shah [22,23], (c) Lazarek and Black [3], (d) Liu and Winterton [24], (e) Tran et al. [6], (f) Lee and Lee [12], (g) Yu et al. [14], and (h) Warrier et al. [15].

$$Nu_4 = 8.235(1 - 2.042\beta + 3.085\beta^2 - 2.477\beta^3 + 1.058\beta^4 - 0.186\beta^5). \quad (8)$$

The first three correlations in Table 3 are popular for determining the two-phase heat transfer coefficient for macro-channels. These correlations include a single-

phase term, h_{sp}, based on turbulent liquid flow prevalent in large channels. The Dittus–Boelter relation used for h_{sp} is a key drawback to using these three correlations for micro-channel flow, where the liquid is almost invariably laminar. The laminar liquid flow is the reason behind using Eqs. (7) and (8) when evaluating h_{sp} in the three macro-channel correlations.

The five remaining correlations in Table 3 were all developed for smaller channels. Notice that correlations 4, 5 and 7 assume heat transfer is dominated by nucleate boiling, while correlations 6 and 8 are based on a form similar to that of macro-channel correlations.

Fig. 5 compares the measured heat transfer coefficient to predictions based on each of the correlations from Table 3. The predictive accuracy of a correlation was measured by the mean absolute error, defined as

$$\mathrm{MAE} = \frac{1}{N}\sum\left[\frac{|\,h_{tp,pred} - h_{tp,exp}\,|}{h_{tp,exp}} \times 100\right]. \qquad (9)$$

Fig. 5 shows all eight correlations yield poor predictions of the present data. The macro-channel correlations generally overpredict the data in the high quality region (region of low h_{tp} values), and underpredict in the low quality region. The three small channel correlations based on nucleate boiling (correlations 4, 5 and 7) and two remaining small channel correlations (6 and 8) all show poor predictions, evidenced by their large MAE values.

6. New correlation

The above assessment of prior correlations points a need for a new tool for accurate prediction of the heat transfer coefficient in refrigerant-cooled micro-channel heat sinks.

As indicated earlier, the compressor of the refrigeration system used in the present study precluded testing at low qualities. In order to both extend the quality range of the new correlation and demonstrate its validity for drastically different fluids, recent micro-channel water data by Qu and Mudawar [18] were examined along with the new R134a data. Fig. 6 shows the variation of the two-phase heat transfer coefficient data with quality for the water data. Interestingly, the water data were obtained by modulating heat flux for a constant mass velocity, while the present R134a data were generated by regulating flow rate for a constant heat flux.

A new technique was sought that could correlate both the water and R134a data based on the Martinelli parameter, X, and account for micro-channel effects not represented in prior correlations. Exhaustive inspection of both the water and R134a databases showed two additional dimensionless parameters were required to adequately correlate all the data. They are the boiling number, Bo, and the liquid Weber number We_{fo}. Figs. 7 and 8 show variations of X^2, Bo and We_{fo} with quality and heat flux for R134a and water, respectively, the latter being more concentrated in the low $x_{e,c}$ region. Overall, these three parameters show different trends for different quality ranges. Therefore, better predictions are possible by dividing the overall quality range into smaller ranges corresponding as closely as possible to the aforementioned flow transitions and data trends.

Three quality ranges provided adequate coverage of both the water and R134a databases. The first is a low quality range of $x_e = 0 - 0.05$. This low heat flux range is most closely associated with bubble nucleation and in-

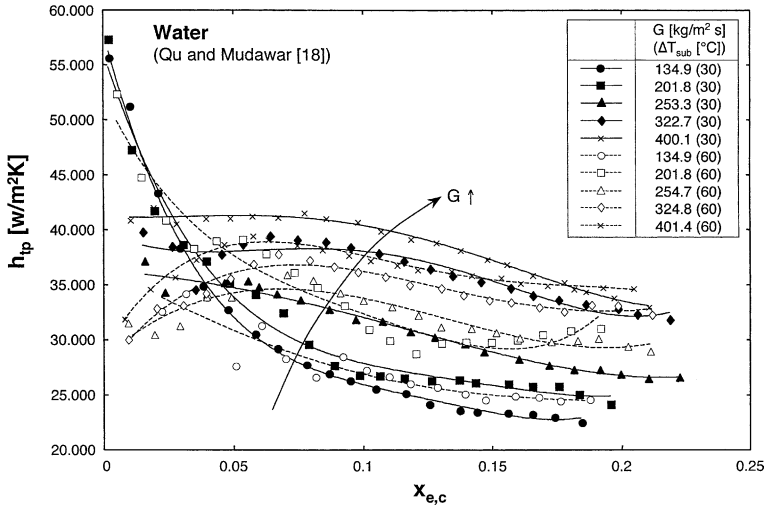

Fig. 6. Variation of local heat transfer coefficient for water (Qu and Mudawar [18]) with thermodynamic equilibrium quality for different mass velocities.

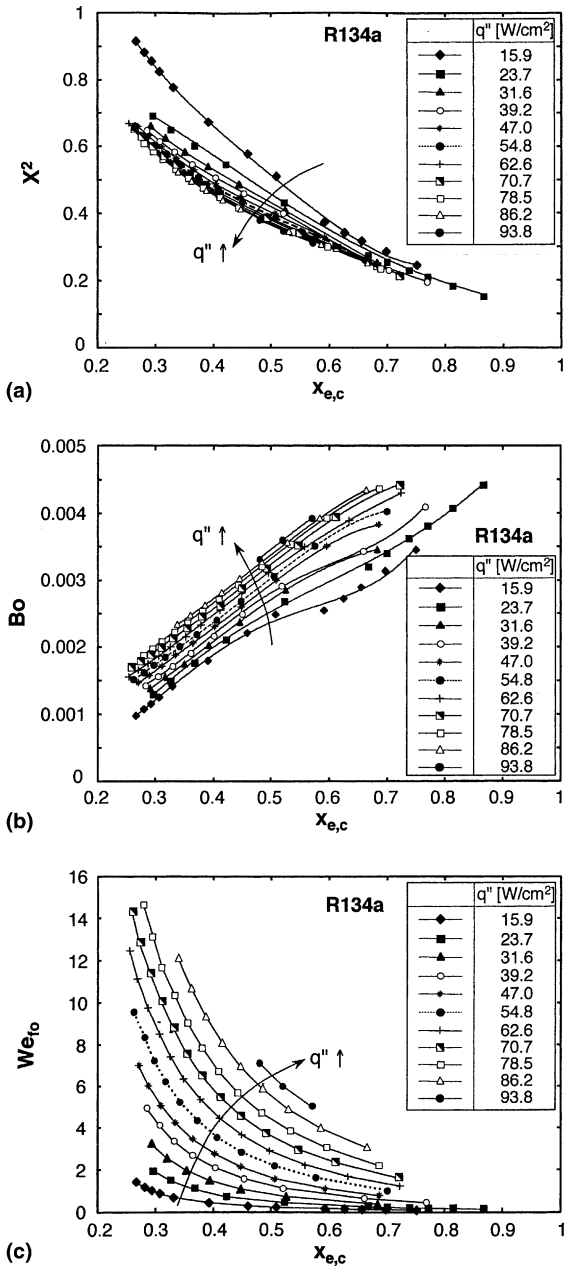

Fig. 7. Variations of (a) Martinelli parameter, (b) boiling number, and (c) Weber number with quality for R134a.

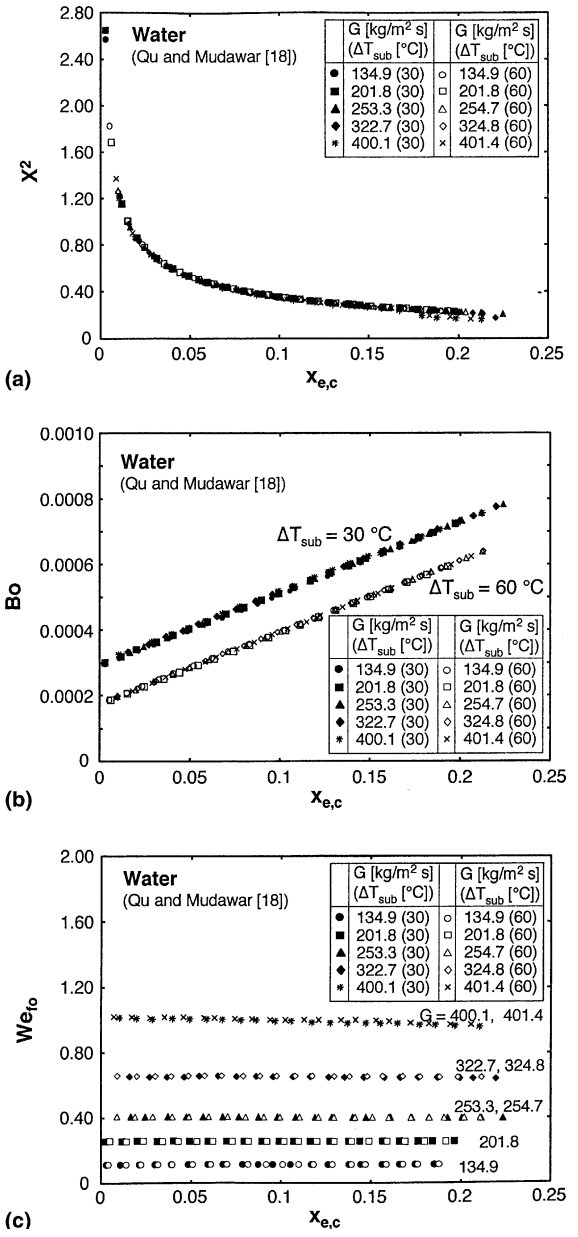

Fig. 8. Variations of (a) Martinelli parameter, (b) boiling number, and (c) Weber number with quality for water (Qu and Mudawar [18]).

cludes 50 water data points and none of the R134a data. These data show rapid and irregular variation of the heat transfer coefficient with quality as shown in Fig. 6. Fig. 8(a) shows the Martinelli parameter in this range is uniquely determined by quality irrespective of flow rate or subcooling, and shows the sharpest decrease with increasing quality.

The second quality range is $x_e = 0.05 - 0.55$, which includes 83 R134a and 157 water data points. This range corresponds mostly to bubbly/slug flow, where the heat transfer data are no longer uniquely determined by the Martinelli parameter, but are sensitive to Bo and We_{fo} as well. The R134a and water data exhibit different trends with quality in this range. While the heat transfer coefficient decreases with increasing quality for both fluids, this decrease is far more pronounced for R134a, Fig. 3, than for water, Fig. 6. Those differences may be partially explained by the different values and trends of Bo

Table 4
Present correlation scheme

x_e	Correlation	Data	MAE (%)
0–0.05	$h_{tp} = 3.856X^{0.267}h_{sp,f}$	50 water data points	11.6
	$X^2 = \frac{(dp/dz)_f}{(dp/dz)_g}, h_{sp,f} = \frac{Nu_3 k_f}{d_h}$		
	$X_{vv} = \left(\frac{\mu_f}{\mu_g}\right)^{0.5}\left(\frac{1-x_e}{x_e}\right)^{0.5}\left(\frac{v_f}{v_g}\right)^{0.5}$		
	$X_{vt} = \left(\frac{f_f Re_g^{0.25}}{0.079}\right)^{0.5}\left(\frac{1-x_e}{x_e}\right)^{0.5}\left(\frac{v_f}{v_g}\right)^{0.5}$		
	$Re_g = \frac{Gx_e d_h}{\mu_g}$		
0.05–0.55	$h_{tp} = 436.48Bo^{0.522}We_{fo}^{0.351}X^{0.665}h_{sp,f}$	83 R134a data points	11.9
	$Bo = \frac{q''}{Gh_{fg}}, We_{fo} = \frac{v_f G^2 d_h}{\sigma}$	157 water data points	
0.55–1.0	h_{tp}=max{$(108.6X^{1.665}h_{sp,g}), h_{sp,g}$}	28 R134a data points	16.1
	$h_{sp,g} = \frac{Nu_3 k_g}{d_h}$ for laminar gas flow		
	$h_{sp,g} = 0.023Re_g^{0.8}Pr_g^{0.4}$ for turbulent gas flow		

and We_{fo} for the two fluids. Comparing Figs. 7(b) and Fig. 8(b) shows drastic differences in the magnitude of Bo, brought about mostly by a much smaller latent heat of vaporization for R134a compared to water. Fig. 7(c) shows far greater We_{fo} values for R134a compared to water, Fig. 8(c), because of the much smaller surface tension of R134a. Furthermore, the large pressure changes in the R134a experiments produced appreciable property changes. Incorporating Bo and We_{fo} in the new correlation is anticipated to account for the drastic property variations that are far more accentuated in a micro-channel than in a macro-channel.

The last quality range is the liquid deficient region of $x_e = 0.55 - 1.0$, consisting of predominantly annular flow and local dryout. This includes 28 R134a data points but none of the water data. Fig. 7(a) shows a convergence of Martinelli number values for different heat fluxes. In this region, the thin annular film is gradually evaporated, sustained only by droplets entrained in the vapor core. Once the majority of droplets are depleted, evaporation results in monotonic thinning and eventual dryout of the liquid film. With this dryout, the heat transfer coefficient is greatly reduced as heat begins to be transferred directly to the vapor. Interestingly, the Martinelli parameter approaches zero as quality goes to unity. Since dryout is followed by convection to vapor, a minimum value for the heat transfer coefficient correlation was set equal to that for convective heat transfer to pure vapor.

Table 4 summarizes the new correlations for the three quality regions. The low and high quality regions are based solely on the Martinelli parameter while the mid range includes the effects of Bo and We_{fo} as well. Overall, convection to liquid is important for both the low and mid quality regions, while convection to vapor becomes important for the high quality region. For the latter, the low viscosity of R134a vapor yields vapor Reynolds numbers corresponding to turbulent flow at high-heat-flux conditions despite the small hydraulic diameter of the micro-channel. Thus, the single-phase vapor term in the high quality correla-

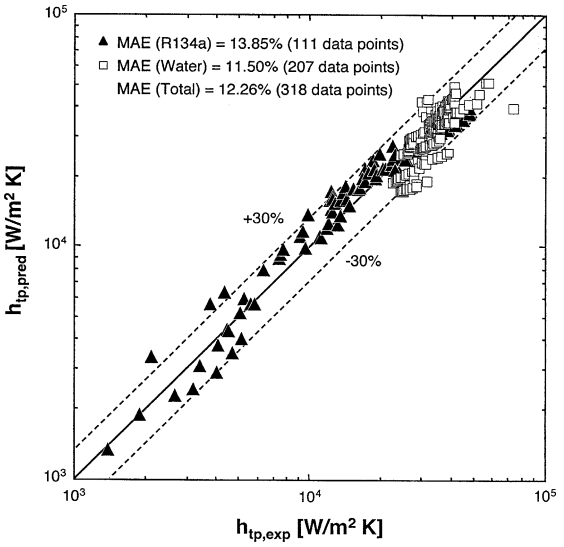

Fig. 9. Comparison of heat transfer coefficient data for R134 and water with predictions based on new correlation scheme.

tion must allow for both laminar or turbulent vapor flow.

Table 4 shows the effect of the Martinelli parameter is important for each of the three quality ranges. The present correlations show the heat transfer coefficient is proportional to the Martinelli parameter raised to a positive exponent, whereas prior macro-channel correlations employ a negative exponent for the same parameter.

Fig. 9 shows excellent agreement between predictions based on the new correlation scheme and both the R134a and water data. An overall MAE of 12.26% indicates excellent predictive capability, especially with most of the data falling within a ±30% error range and capturing the correct data trend.

7. Conclusions

Experiments were performed to explore the heat transfer characteristics of a micro-channel heat sink incorporated as an evaporator in a refrigeration cycle. Flow visualization studies at different quality values were used along with heat transfer coefficient data to develop a new correlation scheme for micro-channel flow that was validated for both R134a and water. Key findings from the study are as follows:

(1) Two-phase heat transfer in micro-channel heat sinks is associated with different mechanisms for low, medium and high quality flows. Bubbly flow and nucleate boiling occur only at low qualities ($x_e < 0.05$) corresponding to very low heat fluxes. High fluxes produce medium quality ($0.05 < x_e < 0.55$) or high quality ($0.55 < x_e < 1.0$) flows (depending on flow rate), where the heat transfer is dominated by annular film evaporation. Because of the large differences in heat transfer mechanism between the three quality regions, better predictions are possible by dividing the quality range into smaller ranges corresponding to these flow transitions.
(2) While the Martinelli parameter commonly used in macro-channel correlations is important to each of the three quality ranges, accurate correlation of data for different coolants requires incorporating the effects of boiling number and Weber number for the medium quality range.
(3) A new three-range two-phase heat transfer coefficient correlation is recommended which shows excellent predictive capability for both R134a and water.

Acknowledgment

The authors are grateful for the support of the Office of Naval Research (ONR) for this research.

References

[1] D.B. Tuckerman, R.F.W. Pease, High-performance heat sinking for VLSI, IEEE Electron Dev. Lett. 2 (1981) 126–129.
[2] J. Lee, I. Mudawar, Two-phase flow in high-heat-flux micro-channel heat sink for refrigeration cooling applications: Part I—Pressure drop characteristics, Int. J. Heat Mass Transfer (in press).
[3] G.M. Lazarek, S.H. Black, Evaporative heat transfer, pressure drop and critical heat flux in a small vertical tube with R-113, Int. J. Heat Mass Transfer 25 (1982) 945–959.
[4] M.W. Wambsganss, D.M. France, J.A. Jendrzejczyk, T.N. Tran, Boiling heat transfer in a horizontal small-diameter tube, J. Heat Transfer 115 (1993) 963–972.
[5] M.B. Bowers, I. Mudawar, High flux boiling in low flow rate, low pressure drop mini-channel and micro-channel heat sinks, Int. J. Heat Mass Transfer 37 (1994) 321–332.
[6] T.N. Tran, M.W. Wambsganss, D.M. France, Small circular- and rectangular-channel boiling with two refrigerants, Int. J. Multiphase Flow 22 (1996) 485–498.
[7] P.A. Kew, K. Cornwell, Correlations for the prediction of boiling heat transfer in small-diameter channels, App. Therm. Eng. 17 (1997) 705–715.
[8] T.S. Ravigururajan, Impact of channel geometry on two-phase flow heat transfer characteristics of refrigerants in microchannel heat exchangers, J. Heat Transfer 120 (1998) 485–491.
[9] Y.-Y. Yan, T.-F. Lin, Evaporation heat transfer and pressure drop of refrigerant R-134a in a small pipe, Int. J. Heat Mass Transfer 41 (1998) 4183–4194.
[10] Z.Y. Bao, D.F. Flectcher, B.S. Haynes, Flow boiling heat transfer of Freon R11 and HCFC123 in narrow passages, Int. J. Heat Mass Transfer 43 (2000) 3347–3358.
[11] S.S. Mehendale, A.M. Jacobi, Evaporative heat transfer in mesoscale heat exchangers, ASHRAE Transactions: Symposia, Dallas, TX, 2000, pp. 445–452.
[12] H.J. Lee, S.Y. Lee, Heat transfer correlation for boiling flows in small rectangular horizontal channels with low aspect ratios, Int. J. Multiphase Flow 27 (2001) 2043–2062.
[13] S. Lin, P.A. Kew, K. Cornwell, Two-phase heat transfer to a refrigerant in a 1 mm diameter tube, Int. J. Refrige. 24 (2001) 51–56.
[14] W. Yu, D.M. France, M.W. Wambsganss, J.R. Hull, Two-phase pressure drop, boiling heat transfer, and critical heat flux to water in a small-diameter horizontal tube, Int. J. Multiphase Flow 28 (2002) 927–941.
[15] G.R. Warrier, V.K. Dhir, L.A. Momoda, Heat transfer and pressure drop in narrow rectangular channels, Exp. Therm. Fluid Sci. 26 (2002) 53–64.
[16] D.S. Wen, Y. Yan, D.B.R. Kenning, Saturated flow boiling of water in a narrow channel: time-averaged heat transfer coefficient and correlations, App. Therm. Eng. 24 (2004) 1207–1223.
[17] X. Huo, L. Chen, Y.S. Tian, T.G. Karayiannis, Flow boiling and flow regimes in small diameter tubes, App. Therm. Eng. 24 (2004) 1225–1239.
[18] W. Qu, I. Mudawar, Flow boiling heat transfer in two-phase micro-channel heat sinks—I. Experimental investigation and assessment of correlation methods, Int. J. Heat Mass Transfer 46 (2003) 2755–2771.

[19] F.P. Incropera, D.P. Dewitt, Fundamentals of Heat and Mass Transfer, fifth ed., Wiley, New York, 2002.
[20] S. Mukherjee, I. Mudawar, Pumpless loop for narrow channel and micro-channel boiling, ASME J. Electron. Packaging 125 (2003) 431–441.
[21] J.C. Chen, Correlation for boiling heat transfer to saturated fluids in convective flow, I & EC Process Des. Develop. 5 (1966) 322–329.
[22] M.M. Shah, A new correlation for heat transfer during boiling flow through pipes, ASHRAE Trans. 82 (1976) 66–86.
[23] M.M. Shah, Chart correlation for saturated boiling heat transfer: equation and further study, ASHRAE Trans. 88 (1982) 185–196.
[24] Z. Liu, R.H.S. Winterton, A general correlation for saturated and subcooled flow boiling in tubes and annuli, based on a nucleate pool boiling equation, Int. J. Heat Mass Transfer 34 (1991) 2759–2766.
[25] R.K. Shah, A.L. London, Laminar flow forced convection in ducts: a source book for compact heat exchanger analytical data, Advances in Heat Transfer, Academic Press, New York, 1978, Supplement 1.